



Deposited via The University of Leeds.

White Rose Research Online URL for this paper:

<https://eprints.whiterose.ac.uk/id/eprint/133002/>

Version: Accepted Version

---

**Article:**

Liu, J, Sui, X, Xu, S et al. (2018) Tailoring the lubricative and electroconductive bifunction properties of NbSe<sub>2</sub> film by controlling the sputtering plasma. Applied Surface Science, 455. pp. 1161-1170. ISSN: 0169-4332

<https://doi.org/10.1016/j.apsusc.2018.06.096>

---

© 2018 Published by Elsevier B.V. This manuscript version is made available under the CC-BY-NC-ND 4.0 license <http://creativecommons.org/licenses/by-nc-nd/4.0/>

**Reuse**

This article is distributed under the terms of the Creative Commons Attribution-NonCommercial-NoDerivs (CC BY-NC-ND) licence. This licence only allows you to download this work and share it with others as long as you credit the authors, but you can't change the article in any way or use it commercially. More information and the full terms of the licence here: <https://creativecommons.org/licenses/>

**Takedown**

If you consider content in White Rose Research Online to be in breach of UK law, please notify us by emailing [eprints@whiterose.ac.uk](mailto:eprints@whiterose.ac.uk) including the URL of the record and the reason for the withdrawal request.

# Tailoring the lubricative and electroconductive bifunction properties of NbSe<sub>2</sub> film by controlling the sputtering plasma

Jinyu Liu<sup>a,b</sup>, Xudong Sui<sup>a,c</sup>, Shusheng Xu<sup>a,d,\*</sup>, Shuaituo Zhang<sup>a,c</sup>, Junying Hao<sup>a,\*\*</sup>

<sup>a</sup> State Key Laboratory of Solid Lubrication, Lanzhou Institute of Chemical Physics, Chinese Academy of Sciences, Lanzhou 730000, China

<sup>b</sup> University of Chinese Academy of Sciences, Beijing 100049, China

<sup>c</sup> Qingdao Center of Resource Chemistry and New Materials, Qingdao 266000, China

<sup>d</sup> Institute of Functional Surfaces, School of Mechanical Engineering, University of Leeds, Leeds, LS2 9JT, UK

\* Corresponding author. Tel.: +86 931 4968236 (Junying Hao)

E-mail address: jyhao@licp.cas.cn (Junying Hao), sxxu@licp.cas.cn (Shusheng Xu).

## Abstract

Transition metal dichalcogenides are well known for their outstanding lubricating property. The special one of the family members, metallic NbSe<sub>2</sub> film, was deposited by sputtering in this study. The microstructure, [electrical conductivity and tribological properties](#) of NbSe<sub>2</sub> films were investigated by energy dispersive X-ray spectroscopy (EDS), X-ray photoelectron spectroscopy (XPS), field emission scanning electron microscopy (FE-SEM), grazing incidence X-ray diffraction (GIXRD), high resolution transmission electron microscopy (HRTEM), [four-probe meter and ball-on-disk tribometer](#). The results showed that the microstructure of NbSe<sub>2</sub> film could be tailored by simply controlling the [sputtering power](#). The suitable power of 180 W promoted to crystal growth of NbSe<sub>2</sub> film with edge plane orientation and formation of columnar structure, which possessed low static [contact electrical resistivity](#) and good adhesive strength on steel substrate. Both the dense and loose films made by lower and higher power, respectively, exhibited the downtrend of contact electroconductive and lubricative properties. [The mechanism was discussed in terms of densification and crystallinity of films and transfer film formed on counterpart surface after sliding friction process](#). This novel NbSe<sub>2</sub> film with low friction and [dynamic contact electrical resistance](#) behaviors was expected to a more feasible candidate for lubricative and electroconductive bifunctional material application.

*Keywords:* NbSe<sub>2</sub> film; nanostructure; bifunction; lubrication; electroconductivity; sputtering plasma

## 1. Introduction

Functional surface modification of the engineering materials is essential for the purpose of enhancing their service reliability. Lots of solid lubricants (transition metal disulfides film (TMDs, or  $MX_2$ : M=Mo, W and Nb, X=S, Se) and anti-wear materials (nitride or carbide ceramics) have been studied and employed to protect the contact surface of the most mechanical systems [with moving components](#) [1,2]. With the development of the integration trend of functional surface, the single-function film could not meet the need of multifunction application. Exploitation of lubricative and electroconductive bifunction films with excellent performance is highly desired for many electromechanical devices with dynamic contact mode, including connectors, relays and [switches, and so on](#). This expected film is also a scientifically interesting topic.

Transition metal disulfides are characterized by a laminar structure and the sliding between basal plane of material occurs easily under a shearing force in dry condition, especially in vacuum, which could exhibit a low friction behavior finally [3,4]. Previously, most of the research works of single-function solid lubricant film for space application were only focused on  $MoS_2$  and  $WS_2$  based films. [However, they possess the intrinsic high contact electrical resistivity \(851  \$\Omega\cdot cm\$  and 144  \$\Omega\cdot cm\$ , respectively\) owing to their large direct band gaps \[5,6\].  \$NbSe\_2\$  is one of the TMDs lubricant families, and the previous investigations has already revealed that  \$NbSe\_2\$  presents robust metallic behaviors with a band crossing the Fermi Level originating from the fully unoccupied \*d\*-character valence of Nb atoms. Thus, the metallic  \$NbSe\_2\$  material has not only low friction behavior but also the excellent electroconductivity \(electrical resistivity of  \$5.35\times 10^{-4} \Omega\cdot cm\$ \) at room temperature \[7\]. The early research on  \$NbSe\_2\$  as the lubricant additive was carried out in the 1960s and the positive cooperation between it and the matrix could optimize the lubricative and electroconductive characteristics for the bulky composite materials \[8,9\]. Recently, the keen interest in low temperature superconducting character of  \$NbSe\_2\$  also has been expressed by up-and-coming physicists \[10\]. Nevertheless, this has not led to further systematic investigation of lubricative and electroconductive bifunction  \$NbSe\_2\$  films so far. \[Similar to or even much better than the traditional  \\$MoS\\_2\\$  and  \\$WS\\_2\\$  films, the solid  \\$NbSe\\_2\\$  should have extensively been used as the bifunctional film on the surface of engineering materials. Therefore, the identification of  \\$NbSe\\_2\\$  compound as a potential lubricative and electroconductive bifunctional film should have opened up a new exciting path for the functional surface modification of engineering materials.\]\(#\)](#)

As compared to the traditional preparation processes of film, such as chemical vapor deposition and pulsed laser deposition, the magnetron sputtering technology has the significant advantages of good uniformity, reproducibility of deposited film and the low damage degree of substrate [11,12]. Therefore, the  $NbSe_2$  film was deposited by using the magnetron sputtering technology in this study. [The motivation of the present work was to investigate the effect of sputtering plasma on microstructure and mechanical properties of  \$NbSe\_2\$  film and its bifunctionality \(excellent lubricative and electroconductive performances\).](#)

## 2. Experimental details

### 2.1 Film deposition

NbSe<sub>2</sub> films were deposited by using radio frequency sputtering technique in a cylindrical chamber with equipped magnetron. The films deposited on the commercial n-type Si (100) wafer substrate were used to the composition, structure and morphology analysis, and those on 9Cr18 steel substrate ( $\Phi$  25 mm  $\times$  4 mm) with surface roughness  $R_a$  less than 30 nm were applied for the mechanical/tribological properties test. Meanwhile, the films on microslide substrate (25 mm  $\times$  25 mm  $\times$  1 mm) were selected for the analysis of film electroconductive property. Firstly, the cleaned substrates by alcohol and acetone were set on the sample holder in the vacuum chamber. Before deposition, the vacuum chamber was evacuated to a background vacuum being superior to  $1.0 \times 10^{-3}$  Pa, and then the substrates were Ar ion etched for 15 min at a bias voltage of -600 V to remove possible adsorbates on the surface. During the film deposition, the sintered NbSe<sub>2</sub> target (99.9%) was sputtered continuously at sputtering power of 120 W, 180 W or 240 W for different films. For comparison, all the film thickness was controlled to be around  $1.4 \pm 0.1$   $\mu$ m. The detailed deposition parameters are listed in **Table 1**.

## 2.2 Composition, structure and properties characterization

The chemical composition of films was analyzed by X-ray photoelectron spectroscopy (XPS, EXCALAB 250Xi) equipped with an Ar ion sputtering gun and a monochromatic Al  $K\alpha$  radiation at pass energy of 29.4 eV under a background vacuum of  $2.0 \times 10^{-7}$  Pa. The XPS spectra of films were referenced to C1s line at 284.8 eV. Their crystallographic analysis was performed on a grazing incidence X-ray diffraction (GIXRD, EMPYREAN) device with Cu  $K\alpha$  radiation (40 kV, 30 mA) in grazing mode ( $1^\circ$ ) and a high resolution transmission electron microscope (HRTEM, Tecnai G2 F20S-Twin) operating at 200 kV. The sample for HRTEM analysis was prepared by a mechanical polishing method and then Ar ion milled at a low angle to sample surface. Film morphology and elemental composition was investigated by a field emission scanning electron microscopy (FESEM, JSM-6701F) attached with an energy dispersive X-ray spectroscopy (EDS). Film surface topography and roughness were analyzed by an atomic force microscope (AFM, Multimode V8).

Film hardness and elasticity modulus were evaluated by the nanoindenter (Nanotest 600). The indentation depth was about 15% of the film thickness to exclude the influence of substrates and five replicate indentations were carried out for each sample. The adhesive strength of the film on steel substrate was measured by a nanoscratch tester (UMT-2MT) with a conical diamond tip of 0.4 mm radius and  $90^\circ$  taper angle. For the scratch test, the loading speed of normal force was 0.01 N/s and the maximum loading force was 2.0 N, and the scratch track length was 5.0 mm. A four-probe meter (RTS-9, 4 PROBES Tech) was employed to evaluate the electroconductive property of film in stationary state. The values of electrical resistivity ( $\rho$ ) of film were calculated by equation of  $\rho = \rho_{\square} * d$ , in which  $d$  represented the thickness of NbSe<sub>2</sub> film.

The friction and wear performances of NbSe<sub>2</sub> films in ambient atmosphere (15~25°C, 20~30% RH) were evaluated using a ball-on-disk reciprocating tribometer (UMT-2MT). The tribological performances in low vacuum atmosphere (15~25°C, 0.1~0.5 Pa) were estimated by a ball-on-disk rotary tribometer (GHT-1000E). The disk was the coated steel substrate and the 9Cr18 steel ball with diameter of 4.0 mm was used as a counterpart. The testing conditions are summarized in **Table 2**. After the friction test, profile images and composition of the wear scar were further analyzed by FESEM and

EDS. The *in-situ* lubricative and electroconductive performances of films were carried out by the ball-on-disk reciprocating tribometer (UMT-2MT). And the dynamic contact electrical resistivity was measured by the build-in resistance sensor on this tribometer. Before the test, the anode of the sensor was connected with indenter of the tribometer and the cathode of it and the bottom of coated steel substrate were joined together by a stationary fixture. A whole circuit completed when the indenter touched the surface of the film on the steel substrate, and the resistance sensor received the resistance signals in real time. The resistance and friction signals could be collected in real time during sliding friction process.

### 3. Results and discussion

#### 3.1 Composition and structure

The elemental composition of NbSe<sub>2</sub> films is listed in Table 1 which were normalized to 100 at. %. It could be noted that with increase of sputtering target power from 120 W to 240 W, the Se/Nb ratio increased from 1.73 to 1.95 and the detected oxygen dropped from high rate of 36.67 at. % to 20.0 at. %. For the sputtered MX<sub>2</sub> (TMDs) films, the ratio of X to M were always lower than stoichiometric ratio of 2 and the oxygen was introduced due to contamination by inevitably residual oxygen-containing substances in the vacuum chamber [7,13]. The Se loss in NbSe<sub>2</sub> film should be mainly attributed to the substitutions of Se by residual active O and preferential resputtering of Se during film deposition process. All the high target power, high working pressure and low strength of accelerating electrical field could raise the plasma density and reduce the mean molecular free path of active particle in dramatic sputtering plasma. Thus, the preferential resputtering of Se atoms in this metastable film declined due to the low energy active particles, and the relatively high Se/Nb ratio was achieved.

The chemical component of the films was further analyzed by XPS, and the typical profiles of the XPS spectra of Nb 3d and Se 3d are shown in Fig. 1. As reported previously, the Nb 3d<sub>5/2</sub> and Nb 3d<sub>3/2</sub> peaks for Nb<sup>4+</sup> in NbSe<sub>2</sub> are located at bonding energy of 203.2 eV and 205.9 eV, and those peaks at 203.6 eV and 206.4 eV for Nb<sup>6+</sup> in NbSe<sub>3</sub> and at 207.3 eV and 210.0 eV for Nb<sup>5+</sup> in Nb<sub>2</sub>O<sub>5</sub>, respectively. The peaks of Se 3d<sub>3/2</sub> and Se 3d<sub>1/2</sub> for Se<sup>2-</sup> in NbSe<sub>2</sub> are located at 52.9 eV and 53.6 eV, and those peaks at 54.2 eV and 55.1 eV for Se<sup>2-</sup> in NbSe<sub>3</sub>, respectively [12,14,15]. It could be found that the surface of the as-deposited NbSe<sub>2</sub> film is consisted of the majority of Nb<sub>2</sub>O<sub>5</sub> and a small amount of NbSe<sub>2</sub> and NbSe<sub>3</sub>, as shown in Figs. 1 (a) and (c). The massive oxide of NbSe<sub>2</sub> based film surface should origin from oxidation of the transportation process and intrinsic existence oxide phase of film itself. To characterize actual chemical components of films, the Ar ion was employed to etch the surface of the as-deposited films for 40 s to eliminate the external influence on chemical composition. After the etching process, the Nb 3d and Se 3d peak were revised by C 1s peak at 284.8 eV. The co-existence of inherent phase NbSe<sub>2</sub>, new components of NbSe<sub>3</sub> and Nb<sub>2</sub>O<sub>5</sub>, as shown in Figs. 1 (b) and (d), should be formed during the growth of film in the sputtering plasma. Tsuneta et al. [16] have found that the chain-like structure NbSe<sub>3</sub> was much easily formed as compared with NbSe<sub>2</sub> during the film growing process because the largest facet of NbSe<sub>2</sub> had six-fold rotational symmetry. Along with the formation of NbSe<sub>3</sub> chains, an array of tiny parallel chains could also merge into a plane and then the NbSe<sub>2</sub> formed after the deselenidation of NbSe<sub>3</sub> phase. While a partial of Nb<sub>2</sub>O<sub>5</sub> appeared due

to the stronger affinity between O and Nb than that between Se and Nb in the active sputtering plasma atmosphere [17]. So it is reasonable for the appearance of three components in this deposited film. Based on the sub-profiles of Nb ( $\text{Nb}^{4+}$  for  $\text{NbSe}_2$  and  $\text{Nb}^{6+}$  for  $\text{NbSe}_3$ ) in the XPS profile, the component ratios of  $\text{NbSe}_2/\text{NbSe}_3$  of the films have been calculated (**Table 1**). The  $\text{NbSe}_2/\text{NbSe}_3$  ratio in the range from 0.85 to 0.96 verified that a partial of  $\text{NbSe}_2$  phase could be formed even in the active Nb, S and O particle plasma atmosphere. This method of depositing  $\text{NbSe}_2$  film would be expected to provide the potential possibilities for its bifunctionality (lubricative and electroconductive performances).

The GIXRD spectra of  $\text{NbSe}_2$  films on the steel substrate are shown in **Fig. 2**. It could be seen that both the films deposited under strong sputtering plasma condition (powers of 180 W and 240 W) mainly exhibit *hcp*- $\text{NbSe}_2$  (002), (101), (103) and (112) diffraction peaks with a preferred orientation of (101) plane. The absence of  $\text{NbSe}_3$  and  $\text{Nb}_2\text{O}_5$  crystal phases indicated that both of them should be amorphous structure. A dramatic change that the diffraction peak intensities dropped to a very low level occurred as the sputtering power was reduced to 120 W. The GIXRD results revealed that the crystallinity of  $\text{NbSe}_2$  film could be adjusted by changing the plasma atmosphere during film growth in vacuum chamber. HRTEM is sensitive to the ordered arrangement of crystal. To further elucidate nano-scale structure of the films, the cross-sectional HRTEM lattice images were performed and the typical results from S2 sample are exhibited in **Fig. 3**. The selected area electron diffraction (SAED) pattern, as shown in **Fig. 3** (a), has continuous rings of  $\text{NbSe}_2$  (002), (101) and (112) planes. In **Fig. 3** (b), the films exhibit a composite structure of nanocrystalline and amorphous phase. The absence of basal plane orientation lattice further proved that the films grew preferentially with  $\text{NbSe}_2$  edge plane orientation although it was always restrained by the amorphous phase nearby. [The result obtained from the HRTEM is well line with the structure information from GIXRD analysis.](#)

The surface and cross-sectional FESEM images of  $\text{NbSe}_2$  films are presented in **Fig. 4**. At low sputtering power of 120 W, [the film mainly exhibits appearance of compact and featureless-like morphology, as shown in Figs. 4 \(a\) and \(d\), but disappearance of the columnar structure which is constantly accompanying with crystal growth of edge plane.](#) The strong sputtering plasma (sputtering power of 180 W) could be contributed to the formation of typical columnar morphology (**Figs. 4** (b) and (e)) which should be mainly caused by sufficient surface diffusion and insufficient bulky diffusion of adatoms. [Moreover, the films had the high growth velocity in the  \$\[hk0\]\$  directions in the high active plasma during film growth \[18\].](#) With further increase of sputtering power to 240 W, the loose characteristics of  $\text{NbSe}_2$  film became much more obvious (**Figs. 4** (c) and (f)). In addition, the surface roughnesses of  $\text{NbSe}_2$  films show an uptrend, from 7.1 nm ( $R_a$ ) at 120 W to 58.2 nm ( $R_a$ ) at 240 W, as shown **Fig. 5**. The high activity of plasma generated by high sputtering power was regarded to be a main factor for the insufficient bulky diffusion of growing film, which finally resulted in the preferential and rapid growth of micro zones. Meanwhile, the anabatic resputtering of growing film by the excessive energetic particles in the plasma would interrupt the sustainable growth of large crystal [19]. [In this study, the sputtering power of 180 W was considered to be the most suitable sputtering plasma atmosphere for the growth of  \$\text{NbSe}\_2\$  film which exhibited optimal crystallization and good uniformity.](#)

### 3.2 Mechanical Properties

To probe the effect of structure evolution on the mechanical properties, the nano-indentation measurement was conducted on NbSe<sub>2</sub> films and the hardness ( $H$ ) and elastic modulus ( $E$ ) results are shown in **Fig. 6**. It could be found that the hardness and elastic modulus of films exhibit a downtrend from 3.4 GPa to 0.8 GPa, and from 66.7 GPa to 23.2 GPa, respectively, as the NbSe<sub>2</sub> films were growing in the rising strength of sputtering plasma bombardment. In generally, the film densification and solution hardening effect, namely the distortion degree of the matrix lattice of film, were considered to be the main influential factor on the film hardness. **The low  $H$  and  $E$  values of the columnar films (S3) were attributed to the loose structure of film with significant porous morphology [20]. The increased density of film (S1) growing in the weak sputtering plasma atmosphere contributed to the improvement of film hardness.** While, the carefully controlling of sputtering plasma by using the source power of 180 W could not only promote the crystallization of the NbSe<sub>2</sub> film but also increase the film density which is need for high hardness and high carrying capacity.

Generally, the adhesive strength and toughness of film were considered to be other main factors impacting on the tribological properties. **Fig. 7** presents the friction force ( $F_x$ ) and friction coefficient (COF) curves of NbSe<sub>2</sub> films on steel substrate tested by using nano-scratcher. The scratching process on films could be defined to be two typical stages: the first good adhesion stage under low applied normal force condition and the second peeling stage of film undergoing high applied normal force. The normal force applied at the critical point between these two stages is defined as the adhesive strength [21]. The S2 film has the highest adhesive strength up to 71 gF. The pits in flaking zone at the scratch scar sides of S1 and S3 film were more serious than that in S2 film. Nevertheless, there are still more regions covered by the residual NbSe<sub>2</sub> film at the end of the scratch scar of S2 film profiling from the robust adhesive strength on steel substrate. In addition, there is also scratch debris around the scar due to film brittleness. The above results revealed that the evolution of NbSe<sub>2</sub> film structure had significant influence on the mechanical properties, which might also determine the lubricative and electroconductive properties during the sliding friction process.

### 3.3 Lubricative and electroconductive bifunctional performance

To well elucidate the electroconductive performance of NbSe<sub>2</sub> film, the contact electrical resistivity ( $\rho$ ) in static state of film coated on insulation glass substrate was measured and the results are shown in **Fig. 8**. It could be found that the  $\rho$  value (up to 15.7  $\Omega\cdot\text{cm}$ ) of S1 NbSe<sub>2</sub> film with low crystallinity was much higher than those of S2 (0.095  $\Omega\cdot\text{cm}$ ) and S3 NbSe<sub>2</sub> films (0.72  $\Omega\cdot\text{cm}$ ), both of which were polycrystal. Previously, Barshilia et al. [22] have revealed that the contact electrical resistivity of Au based coating also increased by two orders of magnitude as a small quantity of hetero-elements was introduced as compared with the pure and well crystallized Au material. The ordered arrangement of NbSe<sub>2</sub> crystal of S2 film could reduce the interference of periodic potential field and scattering process of free electron [23,24]. Thus, the S2 film with relatively high crystallinity possessed the low contact electrical resistivity. However, the loose structure characterized by increased scattering of numerous columnar platelet boundary in S3 film would bring down the Hall mobility and carrier concentration, leading to higher contact electrical resistivity.

**Fig. 9** shows the mean friction coefficient and typical friction coefficient curves of NbSe<sub>2</sub> film on

steel substrate in both ambient (20±2 RH%) and vacuum conditions. The results show that for all the films, the vacuum friction coefficient was ~0.04 while the S2 film shows the longest wear life up to  $3.8 \times 10^5$  cycles. It was 10 and 13 times longer than those of dense S1 film and loose S3 film, respectively. As the work condition was switched into ambient environment, the friction coefficients of S1 and S2 films increased significantly to 0.07~0.08 and the S3 film was worn out quickly, indicating the looser structure NbSe<sub>2</sub> film was more sensitive to humid air than the relatively dense NbSe<sub>2</sub> film. As reported previously, the TMDs films constantly possessed relatively low friction coefficient in moderate environments (vacuum and dry condition) benefiting from the rearranged orientation to basal planes which were parallel to sliding surface induced by friction interaction [25,26]. Thus, as one of TMDs, the wear track of NbSe<sub>2</sub> film should also underwent a recrystallization process from the amorphous phase (S1 film) or crystal orientation transformation process from (101) plane (S2 and S3 film) to (002) plane to achieve low friction. The wear resistance of TMDs film mainly depended on the robust subsurface of wear track that acted as the supporter between the counterparts. The suitable density and occasional introduction of NbSe<sub>3</sub> and Nb<sub>2</sub>O<sub>5</sub> during S2 film growth process would tend to form the mixture phase at subsurface layer of wear track to enhance film wear resistance in the sliding process [11,27]. Based on the research results, the S2 NbSe<sub>2</sub> film with good crystalline and suitable densification exhibited relatively better electroconductive and tribological performances.

Generally, the transfer film formed on counterpart ball surface is one of the important factors that impact the lubricant performance of films. [Fig.10 shows the FESEM images](#) and the corresponding EDS spectra of wear scar on counterpart after sliding of  $1.2 \times 10^4$  cycles in ambient environment. It could be found that the formed transfer film was surrounded by different quantity of wear debris on the counterpart surface for different films. The compact and large transfer film formed by S2 film could be confirmed by the FESEM images and the strong signals of Nb and Se in the corresponding EDS spectrum (as shown in [Fig. 10 \(b\)](#)). In comparison, the wear debris are more considerable and powdered for the S1 and S3 NbSe<sub>2</sub> films, which would go against the formation of effective transfer film and lead to rapidly wear and short wear life [21,28]. The weak signal strength of Nb and Se elements in the EDS spectra of S1 ([Fig. 10 \(a\)](#)) and S3 ([Fig. 10 \(c\)](#)) further verified the inferior quality of transfer film. For this type of oxidation-sensitive film, the loose structure of S3 NbSe<sub>2</sub> film with numerous active edges is more likely to react with environmental moisture to produce hard oxide phase leading to wear severely [29].

To well elucidate the bifunctionality of NbSe<sub>2</sub> film in actual working condition, the *in-situ* lubricative and electroconductive properties of NbSe<sub>2</sub> films on steel substrates were tested by using the UMT-2MT ball-on-disc tester. In order to further comparatively study the bifunctional properties of lubricants, the bare steel substrate and DLC were also measured by the *in-situ* mode. The corresponding the friction coefficient and electrical resistance curves are shown in [Fig. 11](#) and the mean values of them are listed in [Table 3](#). It could be found that the conductor bare steel has high friction coefficient up to 0.67 and the electrical resistance is 13.41 KΩ ([Fig. 11 \(a\)](#)). As shown in [Fig. 11 \(b\)](#), as a lubricant, DLC could achieve relatively stable and low friction coefficient down to 0.205 but the high electrical resistance up to 96.44 KΩ which is not expected as electrical contact film. Much better, the S2 NbSe<sub>2</sub> film possesses not only the extremely low friction coefficient of 0.066 but also low

electrical resistance of 0.37 K $\Omega$  (Fig. 11 (c)), which is unreachable by other non-noble metal film. This excellent low friction and high electrical conduction behaviors of NbSe<sub>2</sub> film would be rapidly terminated as the lubricative layer was worn out on the wear track.

The sputtering plasma atmospheres for the growth of NbSe<sub>2</sub> film correlated with their mechanical, lubricative and electroconductive properties, which should be ascribed to the microstructure variation of films. The careful controlling of sputtering plasma could promote the significant improvement of NbSe<sub>2</sub> crystallinity of film but without negative loose and separated columnar platelets, i.e. increased dense microstructure of film. In this study, the inherent electroconductive performance of NbSe<sub>2</sub> crystal could be well reproduced in the superior NbSe<sub>2</sub> film. The densification of film and solid solution hardening effect by occasional introduction of NbSe<sub>3</sub> and Nb<sub>2</sub>O<sub>5</sub> during film growth process were also considered to be responsible for the hardness enhancement and high carrying capacity of NbSe<sub>2</sub> film. Moreover, the rearrangement of wear track surface layer with basal planes oriented parallel to the surface induced by friction interaction could play a main role on the low friction coefficient [25,27]. On the basis of chameleon principle [30], the non-lubricated NbSe<sub>3</sub> and Nb<sub>2</sub>O<sub>5</sub> would be selectively released from the wear track surface to the subsurface layer in the sliding process, which could tend to form a mixture phase of random NbSe<sub>2</sub>, NbSe<sub>3</sub> and Nb<sub>2</sub>O<sub>5</sub> and acted as the robust support layer for achieving high wear resistance. The effective and compact transfer film formed on the steel counterpart surface was in favor of sustaining the film lubricant action as well as the good electroconductivity in the sliding process. This novel NbSe<sub>2</sub> film with low friction, high wear resistance and low electrical resistance performances prepared by sputtering technology could be considered to be a more feasible candidate for lubricative and electroconductive bifunctional application.

#### 4. Conclusions

NbSe<sub>2</sub> films were deposited by radio frequency magnetron sputtering and the microstructure has been tailored by simply controlling the sputtering power. The presence of new components of NbSe<sub>3</sub> and Nb<sub>2</sub>O<sub>5</sub> during the film growth process should be due to higher stability of Nb element with high valence state in both NbSe<sub>3</sub> and Nb<sub>2</sub>O<sub>3</sub> than that in NbSe<sub>2</sub>. The suitable sputtering power of 180 W promoted to NbSe<sub>2</sub> crystal growth with edge plane orientation and formation of columnar structure. While the low power resulted in amorphization and densification trend of NbSe<sub>2</sub> and the extremely high power led to inferior structure of coarse columnar platelets with high roughness. For S2 NbSe<sub>2</sub> film with optimized crystallinity, the hardness and adhesive strength on steel substrate was up to 3.2 GPa and 71gF, respectively. The S2 NbSe<sub>2</sub> film on insulation glass substrate possessed a quite low static electrical resistivity of 0.097  $\Omega$ ·cm as compared to other non-noble metal films. This superior NbSe<sub>2</sub> film on steel substrate also presented a low friction coefficient of 0.04 and a long wear life of  $3.8 \times 10^5$  cycles in vacuum condition. Moreover, the lubricative and electroconductive bifunctional properties were implemented simultaneously for the thin NbSe<sub>2</sub> film in the *in-situ* test mode, with low friction coefficient of 0.066 and low dynamic contact electrical resistance of 0.37 K $\Omega$ . This method of depositing thin NbSe<sub>2</sub> film should be considered to be potential possibilities for bifunctional performance application in special precision component.

## Acknowledgements

This work was supported by the National Natural Science Foundation of China (grant number 51375471, 51505465) for financial support.

## Reference

- [1] S. Das, M. Kim, J. W. Lee, W. Choi. Synthesis, Properties, and Applications of 2-D Materials: A Comprehensive Review. *Critical Reviews in Solid State and Materials Sciences* 39 (2014) 231-252.
- [2] B. Deepthi, H. Barshilia, K. Rajam, Konchady M. Structural, mechanical and tribological investigations of sputter deposited CrN-WS<sub>2</sub> nanocomposite solid lubricant coatings. *Tribology International*, 2011. 44(12): 1844-1851.
- [3] X. Quan, M. Hu, X.M. Gao, Y.L. Fu. Friction and wear performance of dual lubrication systems combining WS<sub>2</sub>-MoS<sub>2</sub> composite film and low volatility oils under vacuum condition. *Tribology International*, 2016. 99: 57-66.
- [4] A. C. Domask, R. L. Gurunathan, S. E. Mohny. Transition Metal-MoS<sub>2</sub> Reactions: Review and Thermodynamic Predictions. *Journal of Electronic Materials* 44 (2015) 4065-4079.
- [5] I. Williamson, S. Li, A. Correa Hernandez, M. Lawson, Y. Chen, L. Li. Structural, electrical, phonon, and optical properties of Ti- and V-doped two-dimensional MoS<sub>2</sub>. *Chemical Physics Letters* 674 (2017) 157-163.
- [6] S. Z. Butler, S. M. Hollen, L. Cao, Y. Cui, J. A. Gupta, H. R. Gutierrez, T. F. Heinz, S. S. Hong, J. Huang, A. F. Ismach, E. Johnston-Halperin, M. Kuno, V. V. Plashnitsa, R. D. Robinson, R. S. Ruoff, S. Salahuddin, J. Shan, L. Shi, M. G. Spencer, M. Terrones, W. Windl, J. E. Goldberger. Progress, Challenges, and Opportunities in Two-Dimensional Materials Beyond Graphene. *Acs Nano* 7 (2013) 2898-2926.
- [7] Y. Ding, Y. L. Wang, J. Ni, L. Shi, S. Q. Shi, W. H. Tang. First principles study of structural, vibrational and electronic properties of graphene-like MX<sub>2</sub> (M=Mo, Nb, W, Ta; X=S, Se, Te) monolayers. *Physica B* 406 (2011) 2254-2260.
- [8] D. J. Boes, L. E. Moberly. Electrically conductive solid lubricant members and process and apparatus employing them. U.S. Patent 3,300,667 (1963).
- [9] B. B. Chen, J. Yang, Q. Zhang, H. Huang, H. P. LI, H. Tang, C. S. Li. Tribological properties of copper-based composites with copper coated NbSe<sub>2</sub> and CNT. *Materials & Design* 75 (2015) 24-31
- [10] M. B. Alemayehu, M. Falmbigl, C. Grosse, K. Ta, S. F. Fischer, D. C. Johnson. Structural and electrical properties of a new (SnSe<sub>(1.16)</sub>)<sub>(1)</sub>(NbSe<sub>2</sub>)<sub>(1)</sub> polytype. *Journal of Alloys and Compounds* 619 (2015) 861-868.
- [11] A. E. Day, J. S. Zabinski. A parametric study of pulsed laser deposited niobium diselenide thin-film growth. *Thin Solid Films* 238 (1994) 207-212.
- [12] N. D. Boscher, C. J. Carmalt, I. P. Parkin. Atmospheric Pressure Chemical Vapour Deposition of NbSe<sub>2</sub> Thin Films on Glass. *European Journal of Inorganic Chemistry* 2006 (2006) 1255-1259.
- [13] E. Arslan, F. Bülbül, A. Alsaran, A. Celik, I. Efeoglu. The effect of deposition parameters and Ti content on structural and wear properties of MoS<sub>2</sub>-Ti coatings. *Wear* 259 (2005) 814-819.
- [14] B. Zhao, J. Huang, Q. Fu, L. Yang, J. Zhang, B. Xiang. MoS<sub>2</sub>/NbSe<sub>2</sub> Hybrid Nanobelts for Enhanced Hydrogen Evolution. *Journal of The Electrochemical Society* 163 (2016) H384-H387.
- [15] X. H. Zhang, D. Zhang, H. Tang, X. R. Ji, Y. Zhang, G. G. Tang, C. S. Li. Facile synthesis and characterization of hexagonal NbSe<sub>2</sub> nanoplates. *Materials Research Bulletin* 53 (2014) 96-101.

- [16] T. Tsuneta, T. Toshima, K. Inagaki, T. Shibayama, S. Tanda, S. Uji, M. Ahlskog, P. Hakonen, M. Paalanen. Formation of metallic NbSe<sub>2</sub> nanotubes and nanofibers. *Current Applied Physics* 3 (2003) 473-476.
- [17] G. Vacquier, A. Casalot, A. Rolland. Superficial characterization of NbSe<sub>2</sub> single crystals: an Auger electron spectroscopy study. *Materials Science and Engineering* 85 (1987) L9-L12.
- [18] G. Jakovidis, I. M. Jamieson, A. Singh. RF-sputtered MoS<sub>2</sub> film morphology and the imperfection nucleation model. *Surface Review and Letters* 10 (2003) 443-448.
- [19] J. Wang, Y. Xia, E. Wieers, L. M. Stals, X. Zhang, J. P. Celis. Influence of deposition conditions on the crystal structure of MoS<sub>2</sub> coating. *Journal of Materials Science & Technology* 22 (2006) 324-328.
- [20] H. Li, G. Zhang, L. Wang. Low humidity-sensitivity of MoS<sub>2</sub>/Pb nanocomposite coatings. *Wear* 350-351 (2016) 1-9.
- [21] T. Banerjee, A. K. Chattopadhyay. Structural, mechanical and tribological properties of pulsed DC magnetron sputtered TiN-WS<sub>x</sub>/TiN bilayer coating. *Surface & Coatings Technology* 282 (2015) 24-35.
- [22] B. Deepthi, G. Srinivas, P. Kumar, D. V. S. Rao, H. C. Barshilia. Sputter Deposited Nanostructured Au-WS<sub>2</sub> Solid Lubricant Coatings. *Nanoscience and Nanotechnology Letters* 4 (2012) 53-60.
- [23] H. W. Wu, R. Y. Yang, C. M. Hsiung, C. H. Chu. Characterization of aluminum-doped zinc oxide thin films by RF magnetron sputtering at different substrate temperature and sputtering power. *Journal of Materials Science: Materials in Electronics* 24 (2012) 166-171.
- [24] J. Lee, K. N. Hui, K. S. Hui, Y. R. Cho, H.-H. Chun. Low resistivity of Ni-Al co-doped ZnO thin films deposited by DC magnetron sputtering at low sputtering power. *Applied Surface Science* 293 (2014) 55-61.
- [25] S. S. Xu, X. M. Gao, M. Hu, J. Y. Sun, D. S. Wang, F. Zhou, L.J. Weng, W.M. Liu. Morphology evolution of Ag alloyed WS<sub>2</sub> films and the significantly enhanced mechanical and tribological properties. *Surface & Coatings Technology* 238 (2014) 197-206.
- [26] P. D. Fleischauer, R. Bauer. Chemical and Structural Effects on the Lubrication Properties of Sputtered MoS<sub>2</sub> Films. *Tribology Transactions* 31 (1988) 239-250.
- [27] S.S. Xu, L.J. Weng, Y.Z. Liu, K.H. Kang, C.L. Kim, D.E. Kim. Microstructure evolution and enhanced vacuum tribological performance of Ni-doped WS<sub>2</sub> composite coating. *Surface & Coatings Technology* 325 (2017) 81-88.
- [28] B. Deepthi, P. Kumar, G. Srinivas, H. C. Barshilia. High performance nanostructured Cr-WS<sub>2</sub> solid lubricant coatings prepared on mechanically textured substrates. *International Journal of Surface and Engineering* 9 (2015) 466-478.
- [29] G. Weise, N. Mattern, H. Hermann, A. Teresiak, I. Bacher, W. Bruckner, H. D. Bauer, H. Vinzelberg, G. Reiss, U. Kreissig, M. Mader, P. Markschlager. Preparation, structure and properties of MoS<sub>x</sub> films. *Thin Solid Films* 298 (1997) 98-106.
- [30] J. Xu, T.F. He, L.Q. Chai, L. Qiao, X.L. Zhang, P. Wang, W.M. Liu, Selective-releasing-affected lubricant mechanism of self-assembled MoS<sub>2</sub>/Mo-S-C nanoperiod multilayer film sliding in diverse atmospheres, *Physical Chemistry Chemical Physics* 19 (2017) 8161-8173.

**Table captions**

**Table 1.** Film deposition conditions, thickness and chemical composition.

**Table 2.** Sliding friction test conditions of film on steel substrate.

**Table 3.** Comparison of friction coefficient and electrical resistance of different films *in-situ* studio.

**Table 1.**

No.	Sputtering time(min)	Working pressure(Pa)	Bias voltage(V)	Sputtering power(W)	Thickness ( $\mu\text{m}$ )	Se/Nb	NbSe <sub>2</sub> /NbSe <sub>3</sub>	O (at. %)
S1	100	1.0	-100	120	1.3	1.73	0.96	36.67
S2	80	1.0	-100	180	1.4	1.78	0.86	20.74
S3	50	1.5	-80	240	1.5	1.93	0.85	22.91

**Table 2**

Tribometer	GHT-1000E	UMT-2MT
Counterpart	9Cr18 steel ball ( $\Phi$ 4 mm)	9Cr18 steel ball ( $\Phi$ 4 mm)
Load	1 N	1 N
Cycle time	-	40 min
Rotate speed	1000 r/min	300 r/min
Temperature	15~25°C	15~25°C
Environment	0.1~0.5 Pa	101.3 MPa, humidity of 20~30% RH

**Table 3.**

Properties	Steel substrate	DLC film	NbSe <sub>2</sub> film (S2)
Friction coefficient	0.67	0.21	0.066
Electrical resistance (K $\Omega$ )	13.41	96.44	0.37

**Figure captions**

**Fig. 1.** XPS spectra of Nb 3d of S2 NbSe<sub>2</sub> film (a) before and (b) after argon-ion etching, Se 3d of S2 NbSe<sub>2</sub> film (c) before and (d) after argon-ion etching.

**Fig. 2.** GIXRD spectra of NbSe<sub>2</sub> films deposited under different sputtering power.

**Fig.3.** Cross-sectional HRTEM images of S2 NbSe<sub>2</sub> film: (a) selected area electron diffraction (SAED) pattern and (b) morphology of typical zone.

**Fig. 4.** FESEM images of surface morphology of (a) S1, (b) S2 and (c) S3 NbSe<sub>2</sub> films, of cross-sectional morphology of (d) S1, (e) S2 and (f) S3 NbSe<sub>2</sub> films.

**Fig. 5.** AFM images of (a) S1, (b) S2 and (c) S3 NbSe<sub>2</sub> films and (d) surface roughness (*Ra*) of NbSe<sub>2</sub> films

**Fig. 6.** Hardness and elastic modulus of NbSe<sub>2</sub> films.

**Fig.7.** Scratching test curves and typical fracture FESEM morphology images after scratch test for (a) S1, (b) S1 and (c) S3 NbSe<sub>2</sub> films on steel substrate.

**Fig. 8.** Electrical resistivity ( $\rho$ ) of NbSe<sub>2</sub> films on insulation glass substrate.

**Fig. 9.** (a) Average friction coefficient and (b) typical friction curves of NbSe<sub>2</sub> films in ambient environment and (c) typical friction curves of NbSe<sub>2</sub> film in low vacuum condition.

**Fig. 10.** FESEM micrographs and EDS spectra of wear scar on the counterpart ball of (a) S1, (b) S2 and (c) S3 NbSe<sub>2</sub> films.

**Fig.11.** *In-situ* friction coefficient and electrical resistance curves of (a) steel substrate, (b) DLC film on steel substrate and (c) S2 NbSe<sub>2</sub> film on steel substrate.

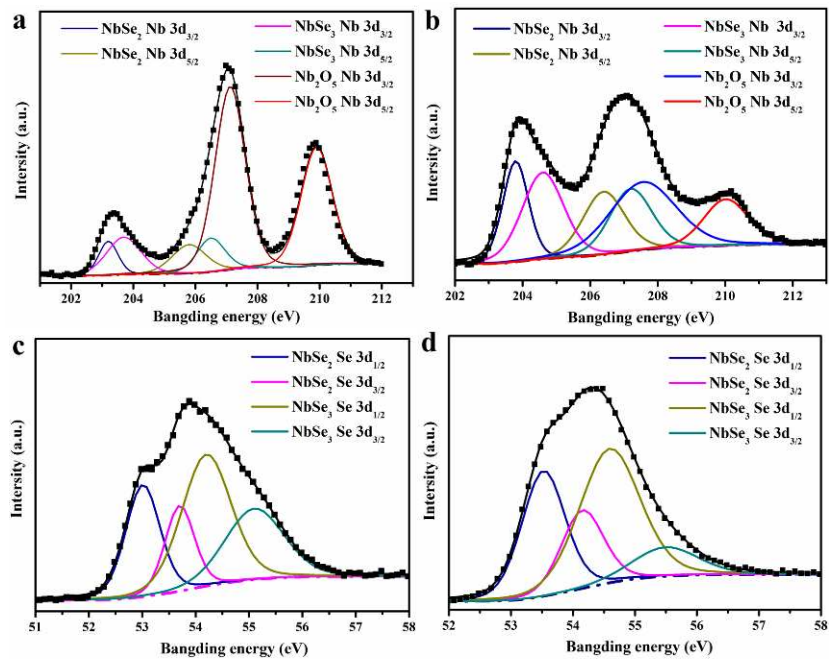


Fig. 1.

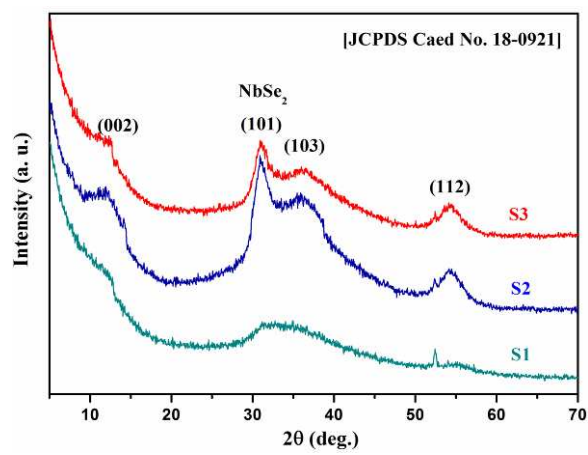
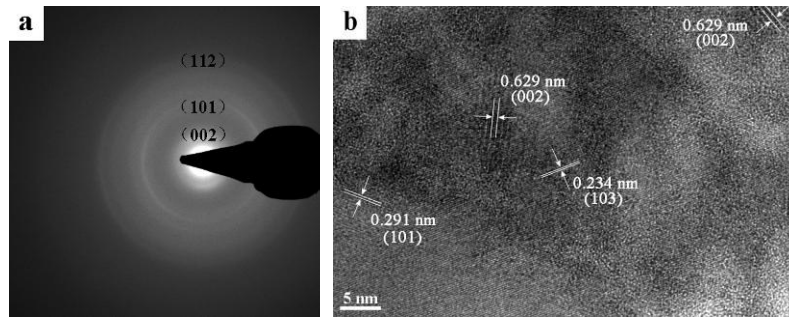
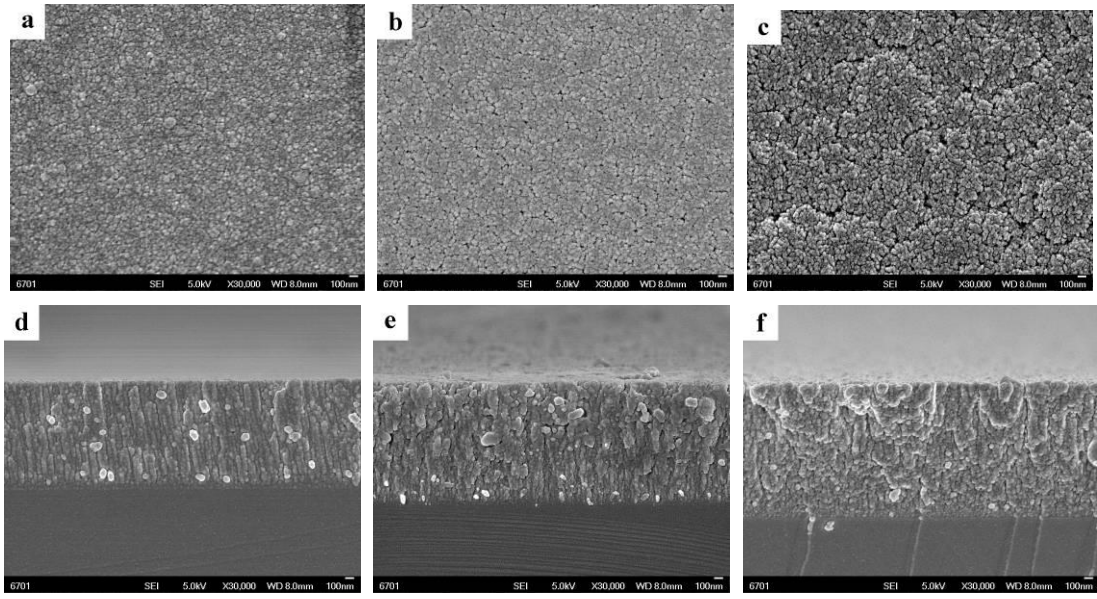


Fig. 2.



**Fig.3.**



**Fig. 4.**

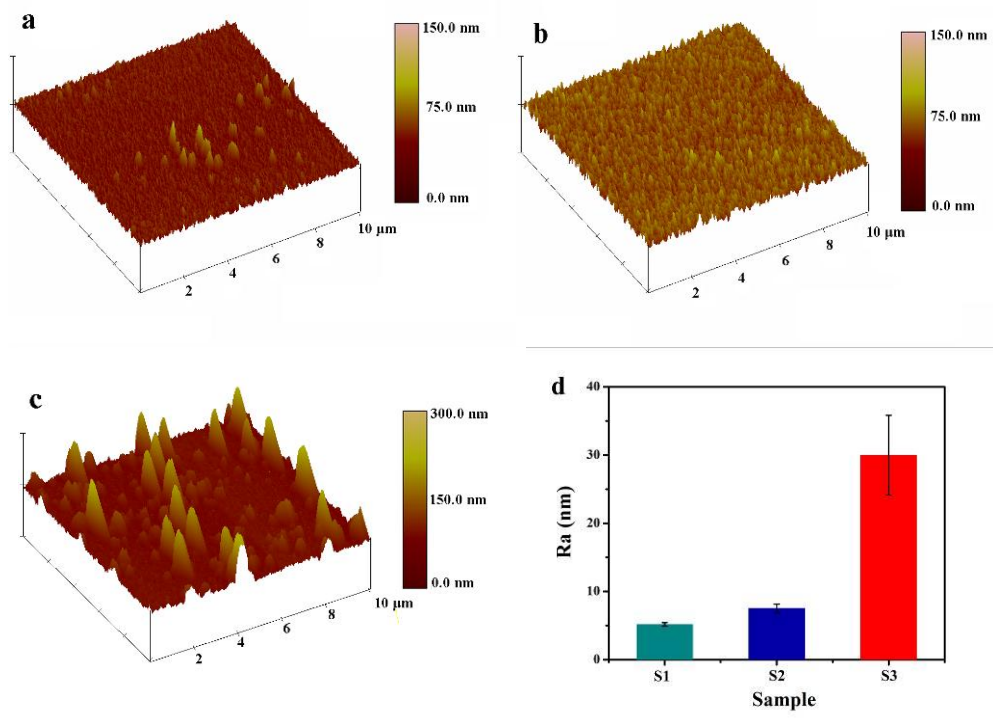


Fig. 5.

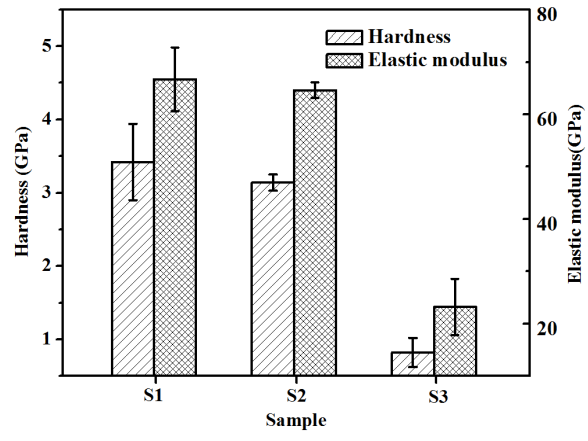


Fig. 6.

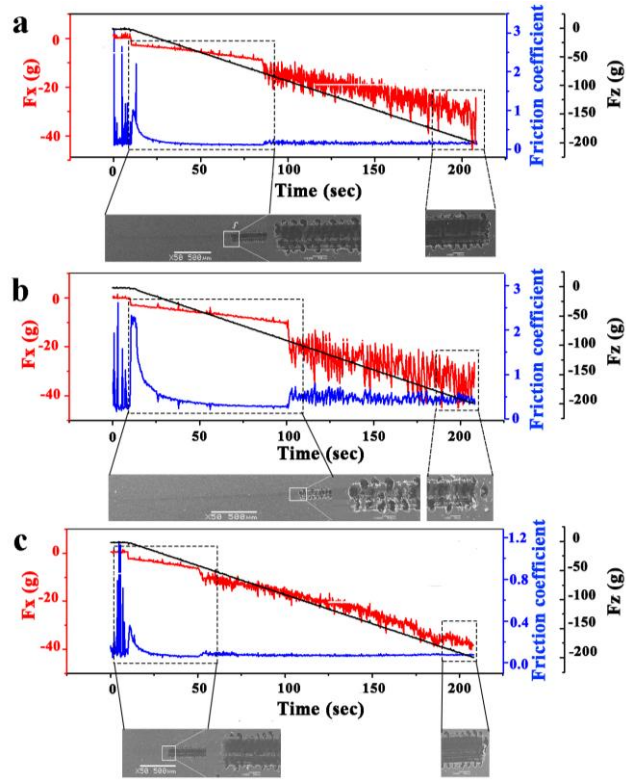
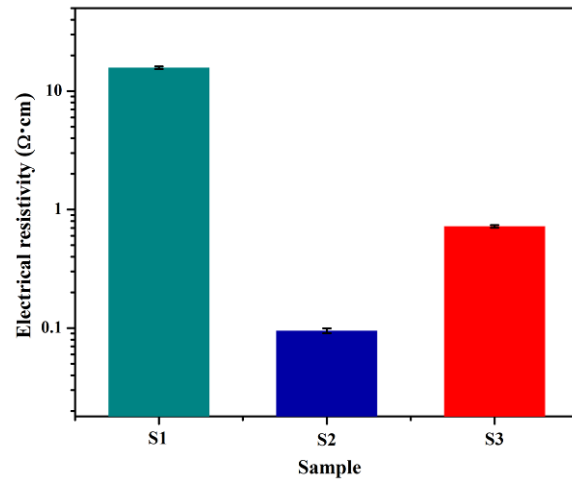
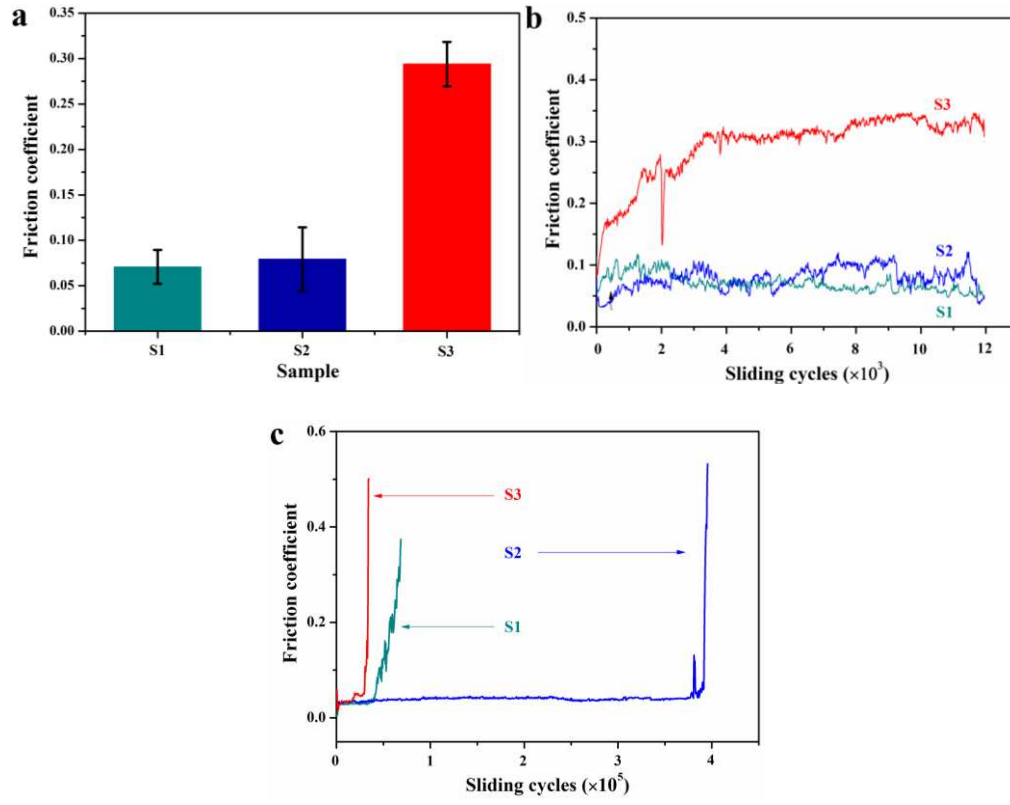


Fig.7.



**Fig. 8.**



**Fig. 9.**

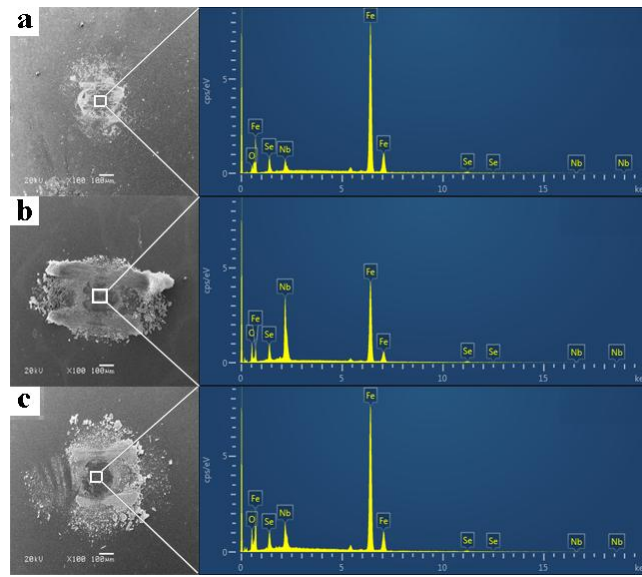


**Fig.10.**

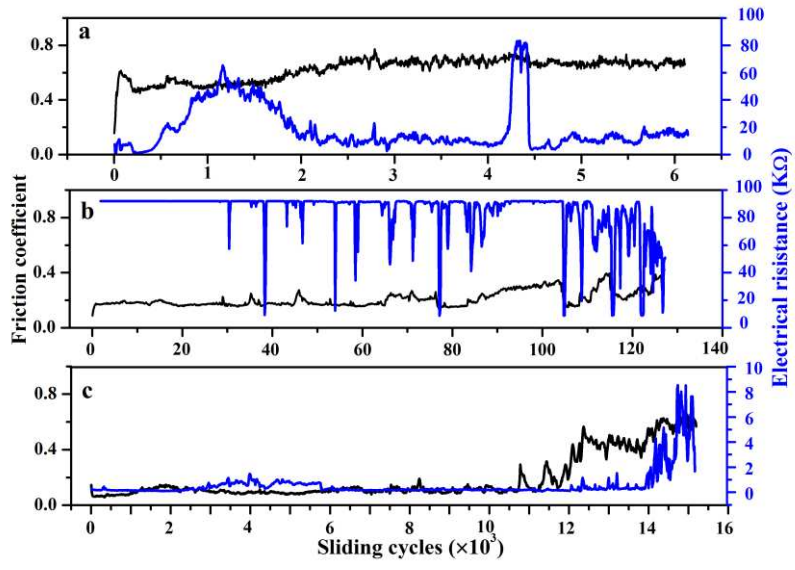


**Fig.11.**